Transactions on Machine Intelligence 5(3) (2022) 174-195

ISSN Online: 2821-1693

Transactions on Machine Intelligence

Journal Homepage: https://tmachineintelligence.ir/index.php/TMI

Design of a Supplementary Controller for STATCOM and Real-Time Parameter Estimation Using Neural Networks in a Hybrid Wind Farm Connected to the Grid

Z. Ghadimi[1,*], A. Karami[2]

[1] Master's student, Department of Electrical Engineering, University of Guilan, Rasht, Iran
[2] Associate Professor, Department of Electrical Engineering, University of Guilan, Rasht, Iran

ARTICLE INFO

Article History:
Received 4 June 2022
Received in revised form 20 July 2022
Accepted 19 September 2022
Available online 20 September 2022

Keywords:
Power Systems, Wind Turbines, SCIG And DFIG Induction Generators, Combined Wind Farm (CWF), STATCOM, PID Controller, Neural Network.

ABSTRACT

In recent years, power systems have encountered numerous challenges, particularly with the growing integration of renewable energy sources. Among these, wind energy has emerged as a clean and cost-effective option, but its impact on power system stability has become a critical concern. This impact largely depends on the type of induction generators used in wind turbines, which are primarily categorized into two types: fixed-speed wind turbines, which typically use squirrel cage induction generators (SCIG), and variable-speed wind turbines, which rely on doubly-fed induction generators (DFIG). A combined wind farm (CWF) leverages the advantages of both generator types. To enhance the dynamic performance of such a wind farm, the integration of compensators is essential. Among these, the Static Synchronous Compensator (STATCOM), a third-generation FACTS (Flexible AC Transmission Systems) device, has gained considerable attention for its effectiveness. In this study, a power system connected to a combined wind farm is designed, with a STATCOM installed at one of its buses. To further improve the damping of system oscillations during faults, a supplementary PID controller is incorporated into the STATCOM structure. The Particle Swarm Optimization (PSO) algorithm is employed to determine the optimal PID controller coefficients. However, as the PSO process can be computationally intensive, an Artificial Neural Network (ANN) is introduced to estimate the PID parameters in real time when system operating conditions change. Simulation results, conducted using MATLAB/Simulink software, demonstrate the effectiveness of the proposed approach, validating its potential to enhance power system stability in the presence of combined wind farms.

1. INTRODUCTION

Over the past two decades, renewable energy sources (RES) have received increasing attention, as conventional energy sources are unable to meet the growing energy demand due to urbanization and industrialization. Environmental pollution caused by conventional energy sources has also pushed utility companies to invest in green

* Corresponding Author: zahraqadimi98@gmail.com
Master's student, Department of Electrical Engineering, University of Guilan, Rasht, Iran

http://dx.doi.org/10.47176/TMI.2022.174

energy instead of fossil fuels [1]. Renewable energy sources have been integrated into the electrical grid to meet energy demand and overcome the disadvantages of conventional energy sources. Among renewable energy sources, wind energy plays an important role due to its low maintenance, lower operating costs, and smaller installation space requirements [2].

In modern power systems, the use of various renewable energy sources (as shown in Figure 1) has accelerated. With advancements in power electronics, the shift toward renewable energy based on power electronic converters, such as wind and solar, has significantly increased. These sources are considered a vital solution for providing clean energy and contributing to a significant reduction in global warming on Earth. Over the past decade (2010-2019), there has been a rapid decrease in the production cost of renewable energy sources, particularly an 82%, 47%, 39%, and 29% reduction in costs for solar photovoltaic (PV), concentrated solar power (CSP), onshore, and offshore wind energy, respectively. Due to this sudden cost reduction, the energy sector has experienced significant growth in solar and wind energy capacity. This growth is evident in Figure 2. Hydropower has long been the largest renewable energy source; however, there has been no significant increase in hydropower in recent years. Thus, PV and wind energy now nearly match hydropower in terms of capacity, as shown in Figure 3 [1].

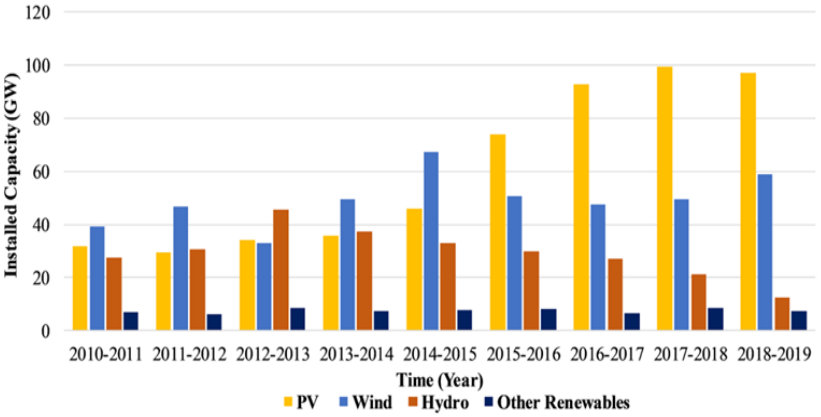

Fig. 1. Classification of Renewable Energy Sources

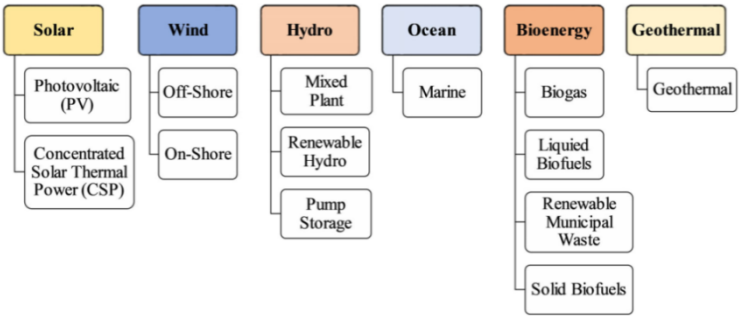

Fig. 2. Global Annual Increase in Renewable Energy

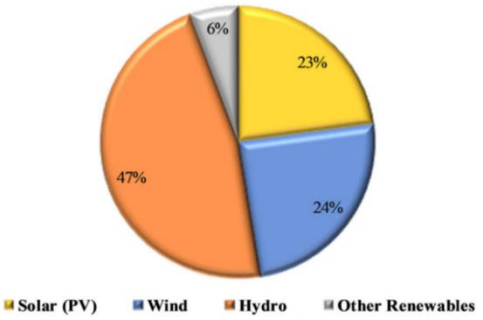

Fig. 3. Share of Renewable Energy Worldwide

In general, wind turbines can be divided into two categories: fixed-speed wind turbines and variable-speed wind turbines. Fixed-speed wind turbines are based on squirrel-cage induction generators (SCIG), while variable-speed wind turbines use doubly-fed induction generators (DFIG). SCIG-based wind turbines are cheaper, but DFIG-based wind turbines provide greater stability. However, in a combined wind farm (CWF) that includes both types of turbines, the advantages of both categories of wind turbines are utilized.

The stability of wind farms is influenced by the exchange of reactive power between the power grid and the wind farms [3]. Reactive power compensators are typically needed to control the voltage level and supply the required reactive power for the wind farm, especially during network disturbances. The Static Synchronous Compensator (STATCOM), one of the most popular components in flexible AC transmission systems (FACTS), is highly useful in simultaneously providing reactive power and supporting the bus voltage of the wind farm [4].

Today, wind energy is widely used in power systems, leading to various challenges such as improving the performance of wind farms, power quality, and system fluctuations under both normal and abnormal conditions. Solving these problems using conventional control methods is complex and difficult. With the advent of computational intelligence techniques such as Artificial Neural Networks (ANN), the parameters of controllers can be rapidly adjusted and tuned according to the operational conditions of the system [5]. In this paper, ANN is used to obtain the optimal parameters of a PID controller to improve the stability performance of a combined wind farm. The effect of the adjusted STATCOM on the performance of the combined wind farm during single-phase, two-phase, and three-phase faults is comprehensively studied. The main goal is to enhance the performance of the combined wind farm using STATCOM and Artificial Neural Networks.

2. LITERATURE REVIEW

The integration of renewable energy sources, particularly wind farms, into the power grid has introduced new challenges related to voltage stability and dynamic response. The Static Synchronous Compensator (STATCOM) has been widely investigated as an effective solution for enhancing grid stability and mitigating power fluctuations. Research by Liu et al. [6] highlights the impact of grid strength and Phase Locked Loop (PLL) parameters on the small-signal stability of wind farms, suggesting that supplementary controllers for STATCOMs can significantly enhance system resilience. Similarly, Wang and Hsiung [7] explored the role of STATCOM-based voltage control in offshore wind farms, demonstrating its effectiveness in improving dynamic stability. Additionally, Zhang et al. [8] proposed fuzzy-logic-based frequency controllers for hybrid wind-storage systems, emphasizing the potential of intelligent control strategies in optimizing power system performance.

The integration of machine learning techniques in power system control has been a growing area of research. Alimi et al. [9] reviewed various machine learning applications for power system stability, underscoring their ability to enhance real-time monitoring and decision-making. Wang et al. [10] introduced a hybrid model-driven and data-driven approach for frequency stability assessment, showing that neural networks can play a crucial role in adaptive control strategies. Moreover, Mokhtari and Aminifar [11] explored anomaly detection methods in power grids using machine learning, highlighting the importance of cybersecurity in modern energy management. These studies collectively suggest that leveraging machine learning for real-time parameter estimation in STATCOM control can significantly improve grid stability and operational efficiency.

Despite these advancements, several research gaps remain. While STATCOMs have been extensively studied for voltage and frequency regulation, the integration of real-time parameter estimation techniques, particularly through deep learning and reinforcement learning, requires further exploration. Arya et al. [12] investigated PSO-based damping controllers for wind farms, indicating the potential of optimization algorithms in enhancing grid resilience. Additionally, Hasanien and El-Fergany [13] proposed a symbiotic organism's search algorithm for automatic generation control, further emphasizing the role of intelligent control methods in improving power system dynamics. Future research should focus on the practical implementation of these advanced control strategies through real-world validation and interdisciplinary approaches to enhance the robustness of hybrid wind farms connected to the grid.

3. SYSTEM MODELING

2.1. Modeling of Induction Generator (IG)

Mathematical modeling of induction generators has been a common feature in all the papers dealing with wind energy. Researchers have used it as an introduction to their work. Figure 4 shows the equivalent circuit of the induction generator, in which conventional symbols are used [14].

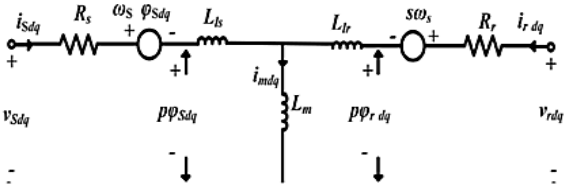

Fig. 4. Equivalent Circuit of the Induction Generator

In general, induction generators can be divided into two categories: squirrel-cage induction generators (SCIG) and doubly-fed induction generators (DFIG).

The rotor voltage of SCIG is zero because the rotor is short-circuited, and as shown in Figure 5, there is no connection between the SCIG rotor and the power grid. In contrast, the rotor of DFIG has a voltage because it is a wound rotor type. As shown in Figure 6, power from the DFIG rotor is transferred to the grid via an AC/DC/AC converter [5].

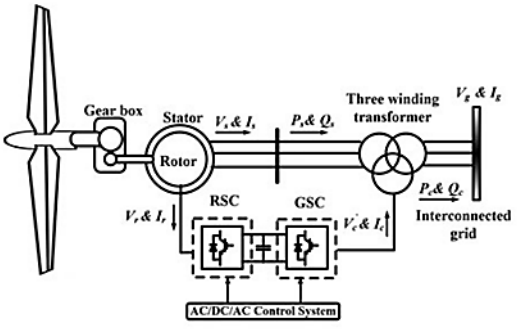

Fig. 6. Schematic Diagram of DFIG Connected to the Grid

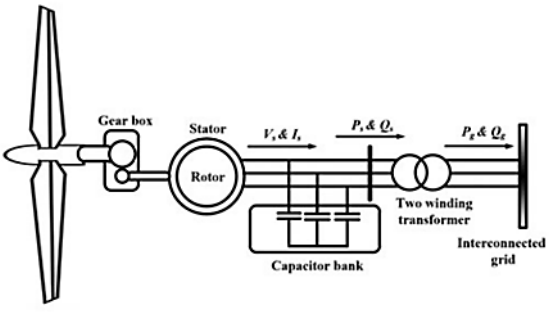

Fig. 5. Schematic Diagram of SCIG Connected to the Grid

2.2. Modeling of Wind Turbine

The power of wind turbines is a fraction of the total energy stored in the wind and can be expressed by equations (1) to (4):

$$P_{wt} = \frac{1}{2}\rho A v^3 C_p \quad (1)$$

$$C_p = 0.517\left(\frac{116}{\lambda_i} - 0.4\beta - 5\right)e^{\frac{-0.0068}{\lambda_i}} + 0.006 \quad (2)$$

$$\frac{1}{\lambda_i} = \frac{1}{116}\left(\frac{1}{\lambda+0.08\beta} - \frac{0.035}{\beta^3+1}\right) \quad (3)$$

$$\lambda = \frac{\omega_r l_b}{v} \quad (4)$$

Where C_p is the power coefficient, which is a function of the tip speed ratio λ and the pitch angle β, v is the wind speed, ω_r is the rotor speed, A is the swept area of the blades in square meters, l_b is the blade length or rotor radius, and ρ is the air density, which is equal to 1.22 kg/m³ [4].

2.3. Modeling of STATCOM

STATCOM is one of the most important and well-known FACTS devices, used for improving the voltage profile. STATCOM, meaning Static Synchronous Compensator, is also known as a static synchronous condenser. It is essentially a voltage regulator device used in AC power systems. Its main design is based on a Voltage Source Converter (VSC). STATCOM is connected in parallel with the transmission line at the point of connection to regulate the voltage. The schematic diagram of STATCOM and its equivalent circuit are shown in Figure 7. As shown in this figure, STATCOM is connected in parallel with the bus of an electrical network and through a coupling transformer. The coupling transformer is connected to a DC bus via the Voltage Source Converter (VSC) [5].

As shown in Figure 7-b, the injected voltage (V_{inj}) of the STATCOM is transferred to the network to regulate the grid voltage (V_g) through X_{Sh}, which represents the reactance of the coupling transformer and VSC. The active and reactive powers transferred can be calculated as follows:

In the context of this section, the STATCOM (Static Synchronous Compensator) is being described as a key device for improving voltage stability in an electrical grid, with its integration with the transmission system and the role of the coupling transformer. The next part of the text seems to introduce the formulas for active and reactive power calculations in the STATCOM system.

$$P = \frac{V_g V_{inj} \sin\delta}{X_{Sh}} \quad (5)$$

$$Q = \frac{V_g\left(V_g - V_{inj}\cos\delta\right)}{X_{Sh}} \quad (6)$$

In steady state, V_{inj} is produced by the VSC in phase with V_g, which indicates that δ=0, P=0, and the reactive power Q is transferred to the grid according to the relationship (7) [3].

$$Q = \frac{V_g\left(V_g - V_{inj}\right)}{X_{Sh}} \quad (7)$$

From the above equation, it can be concluded that the operating condition (operating point) of the STATCOM depends on the values of V_{inj} and V_g. When V_g is greater than V_{inj}, STATCOM absorbs reactive power from the grid, and when V_{inj} is greater than V_g, it injects reactive power into the grid [2].

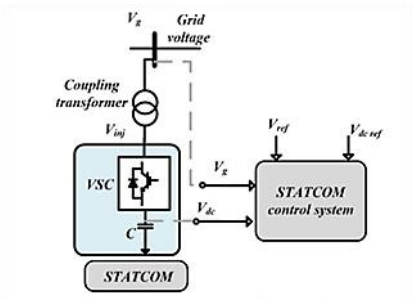

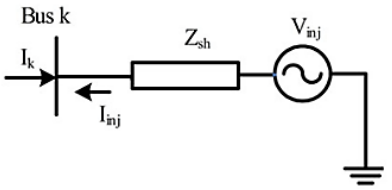

B - Schematic diagram of STATCOM A - Equivalent circuit of STATCOM

Fig. 7. Basic operation of STATCOM

3. PRINCIPLES OF DESIGNING A HYBRID WIND FARM CONNECTED TO THE POWER SYSTEM AND PERFORMANCE EVALUATION

The system studied in this paper consists of two parts: the power system and the wind farm. To simulate the wind farm, Simulink, a component of Matlab software, has been used. Matlab provides the ability to implement the system in Simulink, utilizing pre-built blocks to analyze the dynamic performance of the system in the face of electrical and mechanical faults and how it stabilizes. In this section, the power system connected to the wind farm, including Squirrel Cage Induction Generators (SCIG), is first implemented, and then by adding Doubly Fed Induction Generators (DFIG), the system's performance is enhanced, thereby studying the combined wind farm.

3.1. Simulation of the Power System Connected to the Wind Farm Including Squirrel Cage Induction Generators (SCIG)

For the design of the wind farm, certain blocks in the Simulink environment are required, which will be explained below.

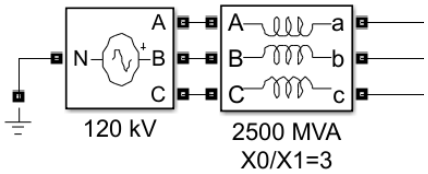

Fig. 8. Voltage Source Block and Mutual Inductance Between Phases in Simulink Environment

As shown in Figure 8, a 3-phase voltage source with a voltage of 120 kV is used to model the power grid. This block is connected to another block with an apparent power of 2500 MVA and a ratio of x0x1=3\frac{x_0}{x_1} = 3. In fact, this block is used to model the mutual inductance between the phases.

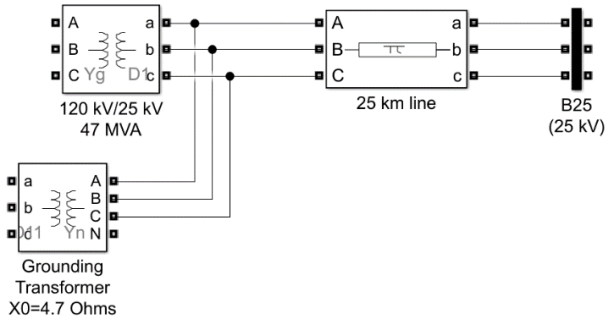

Fig. 9. Transformer and transmission line block in the Simulink environment

In Figure 9, two blocks are shown for modeling the transformer. The first block is a three-phase transformer for converting a voltage of 120 kV to 25 kV, with an apparent power of 47 MVA and a primary Yg configuration and a secondary delta (D1) configuration. The second block is a grounding transformer with X0 = 4.7 ohms and a primary Yn configuration and a secondary delta (D11) configuration. These two transformers are then connected to a 25-kilometer long three-phase transmission line, which is modeled as a π-block.

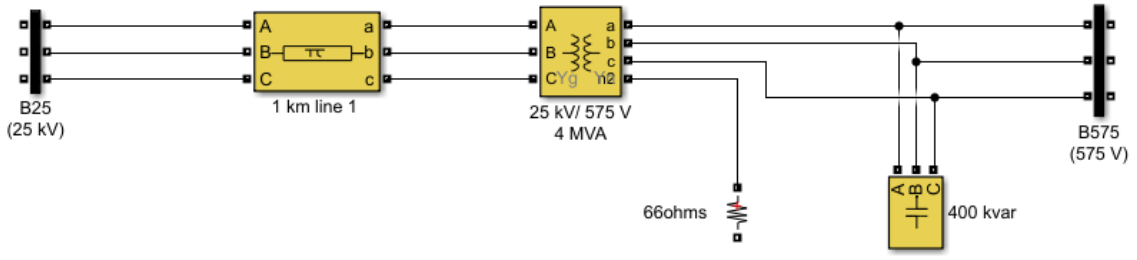

Fig. 10. Transformer, Transmission Line, and Parallel Capacitor Block in the Simulink Environment

In Figure 10, a step-down transformer is used to convert and reduce the voltage from 25 kV to 575 V. The apparent power of this transformer is 4 MVA, with a primary Yg configuration and a secondary Yn configuration. After the block corresponding to the step-down transformer, a parallel capacitor block with a power rating of 400 Kvar is used.

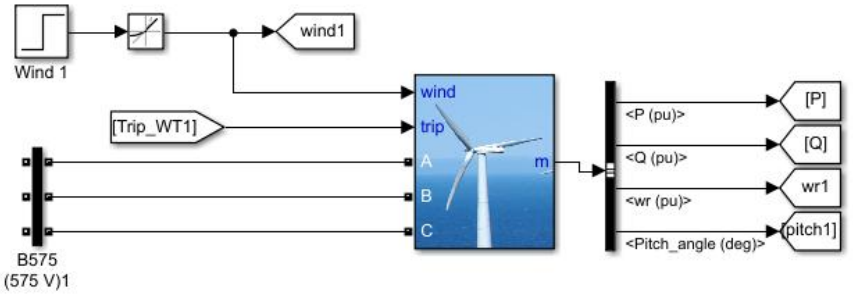

Fig. 11. Squirrel Cage Wind Turbine Block in Simulink Environment

At the end, the second part of the system (the wind turbine) is modeled as shown in Figure 11. The inputs to the wind turbine are wind, trip signal, and transmission line. The outputs of the wind turbine include active and reactive power, rotor speed (wr), and pitch angle. Figure 12 also shows the protective section of the system.

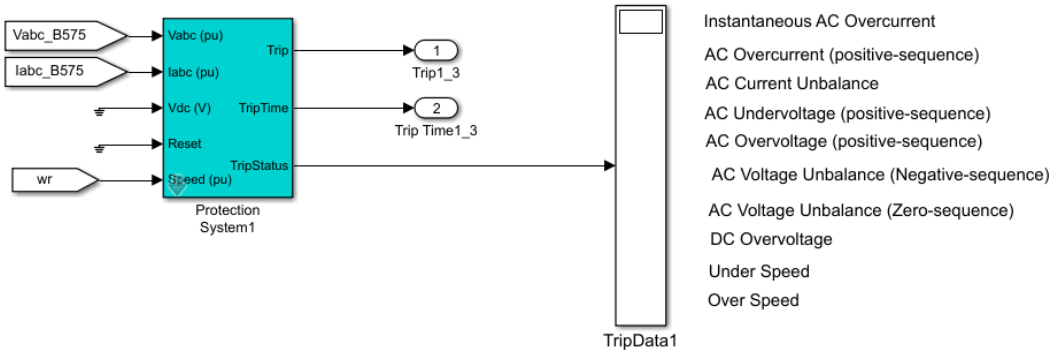

Fig. 12. Protective system block of the wind turbine in the Simulink environment.

Figure 13 shows the power system connected to the squirrel-cage wind farm modeled in Simulink. In this figure, a wind farm with a capacity of 9 megawatts is considered.

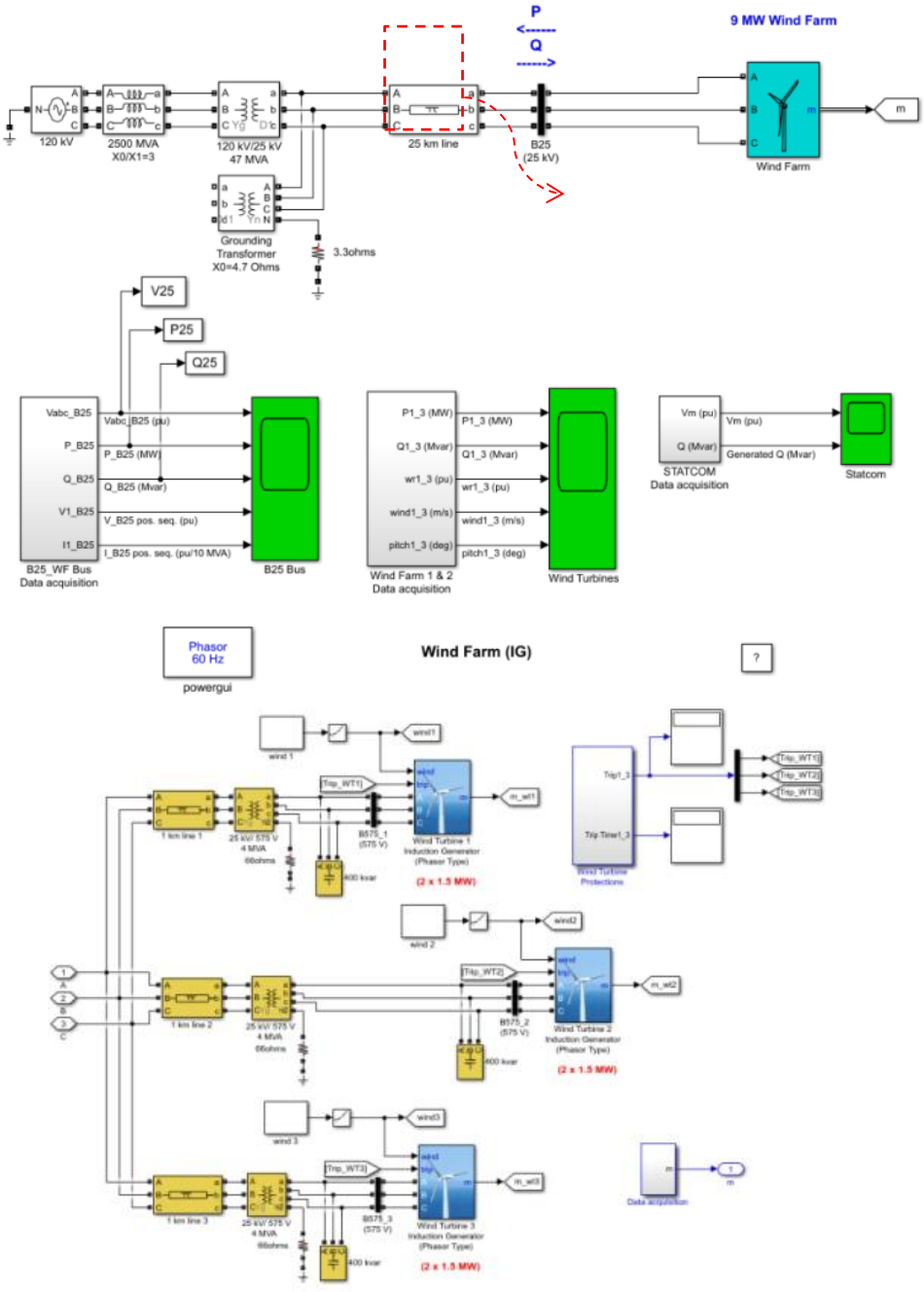

Fig. 13. Simulation of the power system connected to a 9 MW wind farm including squirrel-cage wind turbines (SCIG) in Simulink.

3.2. Simulation of the power system connected to a hybrid wind farm with SCIG and DFIG turbines

Figure 14 shows a hybrid wind farm connected to the grid (power system). In this system, the capacity of the squirrel-cage wind turbine is assumed to be twice that of the doubly-fed induction generator (DFIG) wind turbine. The steady-state waveform of the output active power at the 25 kV bus and corresponding to both the SCIG wind farm and the hybrid wind farm are compared in Figure 15.

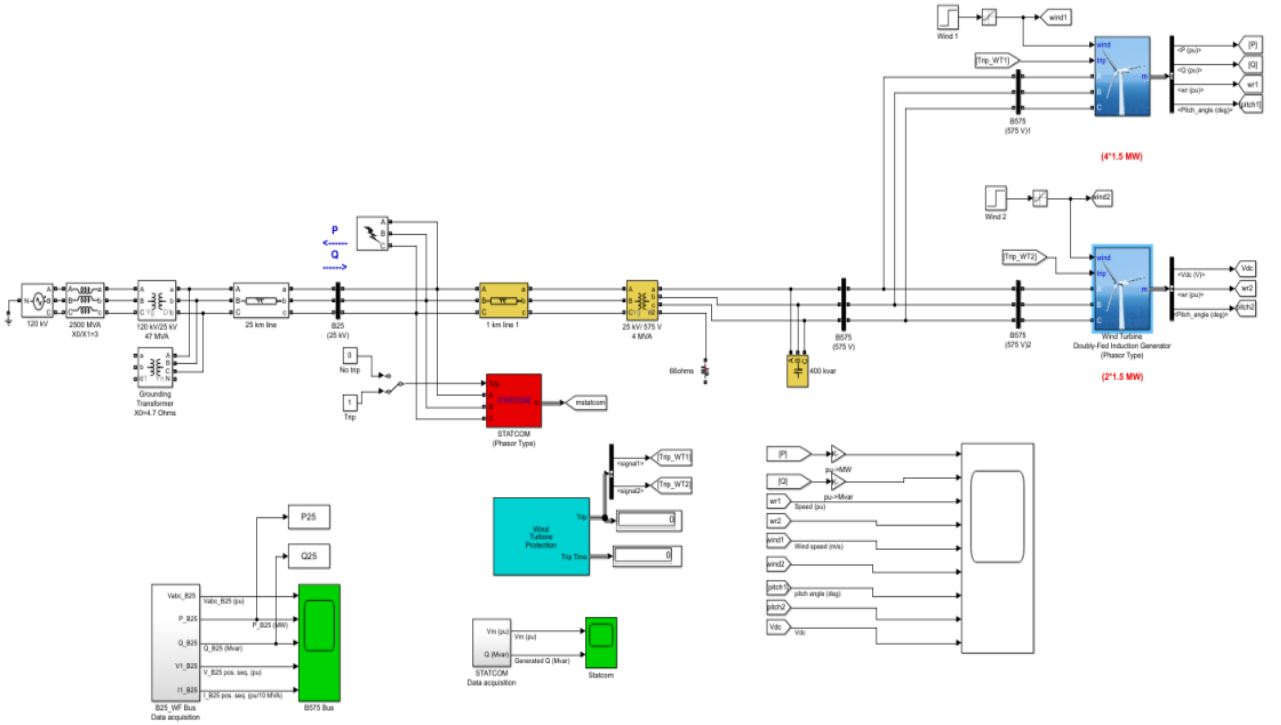

Fig. 14. Simulation of the power system connected to a 9 MW hybrid wind farm including Squirrel Cage Induction Generators (SCIG) and Doubly Fed Induction Generators (DFIG) wind turbines in Simulink.

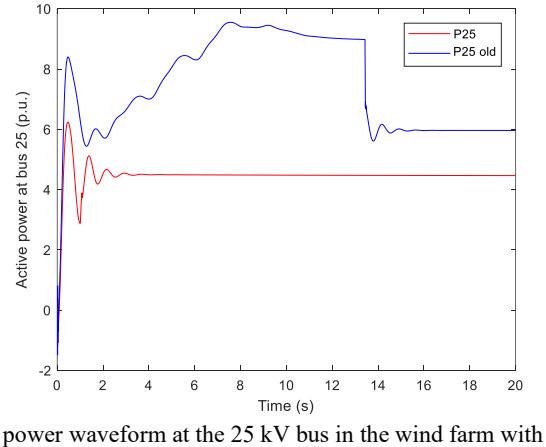

Fig. 15. Comparison of the active power waveform at the 25 kV bus in the wind farm with SCIG and the hybrid wind farm in steady state.

3.3. The Necessity of Using STATCOM

In the studied system, an analysis was conducted to determine whether STATCOM is necessary, and if so, under what conditions STATCOM should be activated. To answer this question, it's important to note that two types of faults can occur in the system:

1. **Mechanical Faults**: These are disturbances introduced into the system, and in this case, changes in wind speed are considered as mechanical faults.
2. **Electrical Faults**: These refer to faults such as single-phase, two-phase, and three-phase faults (to ground).

The electrical fault was applied to the system, and it was observed that STATCOM has a positive impact on electrical faults but no effect on mechanical faults. The results obtained are shown in the following figures. All faults were applied at the 25 kV bus at 15 seconds after simulation started and lasted for 0.1 seconds. This analysis shows that while STATCOM can help mitigate voltage instability caused by electrical faults, it doesn't have an impact on mechanical disturbances such as changes in wind speed, which do not directly affect the system's voltage profile in the same way.

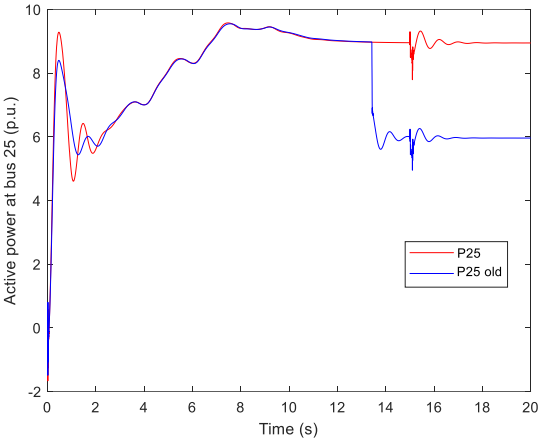

Fig. 16. Active power waveform of the 25 kV bus during a single-phase-to-ground fault with and without the presence of STATCOM in the SCIG wind farm.

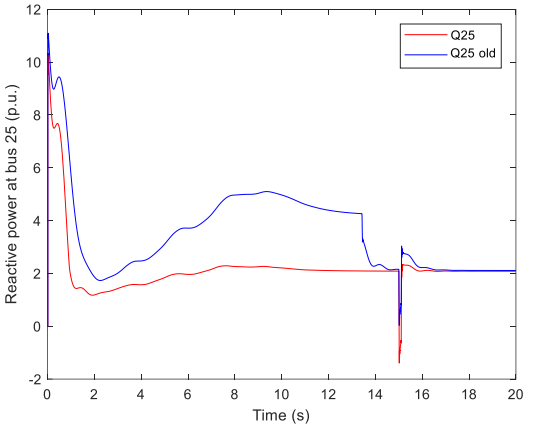

Fig. 17. Reactive power waveform of the 25 kV bus during a single-phase-to-ground fault with and without the presence of STATCOM in the SCIG wind farm.

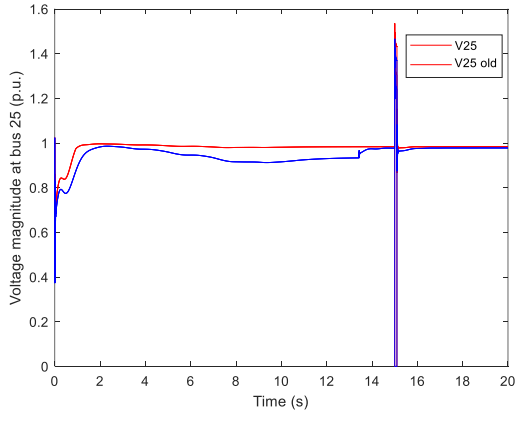

Fig. 18. Voltage waveform of the 25 kV bus during a single-phase-to-ground fault with and without the presence of STATCOM in the SCIG wind farm.

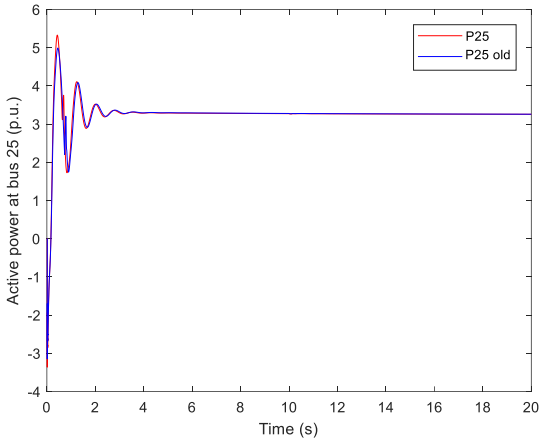

Fig. 19. Active power waveform of the 25 kV bus during a single-phase-to-ground fault with and without the presence of STATCOM in the hybrid wind farm.

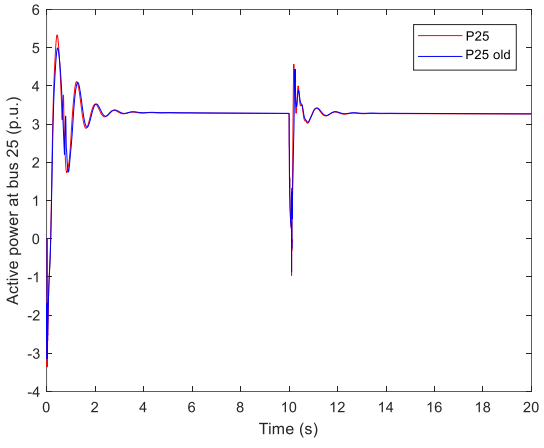

Fig. 20. Active power waveform of the 25 kV bus during a two-phase-to-ground fault with and without the presence of STATCOM in the hybrid wind farm.

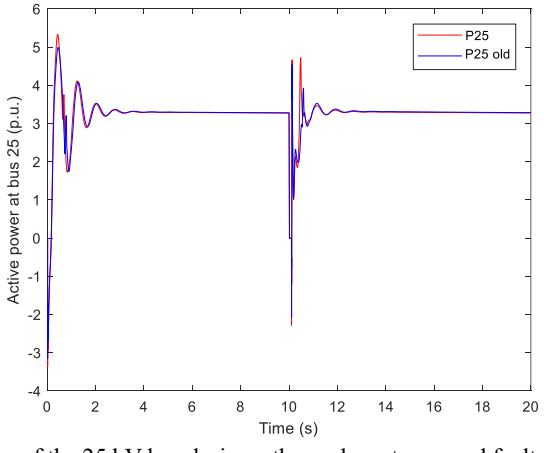

Fig. 21. Active power waveform of the 25 kV bus during a three-phase-to-ground fault with and without the presence of STATCOM in the hybrid wind farm.

As shown in Figures 19 to 21, STATCOM has had a limited impact on the performance of the power system connected to the hybrid wind farm. Therefore, to improve the system's behavior after fault occurrence, an additional controller for STATCOM has been used, which will be explained in the next section.

3.4. Improvement of System Performance by Adding a Supplemental Controller to STATCOM

By adding a PID controller to the reference voltage (Vref) section related to the STATCOM settings, the power system performance can be improved. The overall structure of this supplemental controller is shown in Figure 22. The input signal for this supplemental controller is essentially the speed deviation of an induction motor present in the system, as detailed in Figure 23. This speed deviation, after passing through a washout stage, enters the main PID controller. Additionally, the value w0=0.9933w_0 = 0.9933w0=0.9933 has been considered, and the washout stage is assumed to be 10S/(10S+1)10S / (10S + 1)10S/(10S+1).

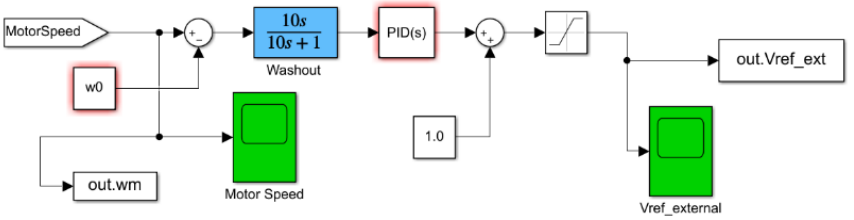

Fig. 22. Supplemental PID Controller for STATCOM

In Figure 23, a load complex with a nominal power of 2 MVA is shown, which is fed by a wind farm. The details of this load complex are also provided in Figure 23. This load consists of two main components: a dynamic load, denoted as **PLD**, and a static load, denoted as **PLS**.
The mentioned dynamic load is essentially an induction (asynchronous) motor with a nominal power of 1.68 MW, a power factor of 0.93, and a line voltage of 2300 volts. The static load is a constant power load with a nominal power of 200 kW, supplied at a voltage of 2300 volts and a frequency of 60 Hz.

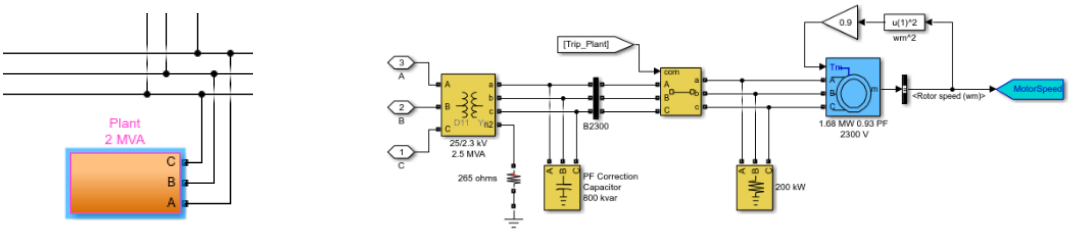

Fig. 23. Block Diagram of a Load Complex in the Simulated System

It should be noted that the transfer function of the main PID controller, as shown in Figure 22, is as follows:

$$PID(s) = K_p + \frac{K_i}{s} + K_d s \tag{8}$$

Where K_p,K_i, and K_d represent the coefficients of the proportional, integral, and derivative terms of the PID controller, respectively. The steady-state waveform of the active power of the hybrid wind farm, in the presence and absence of the supplemental controller for STATCOM, and for several selected values of the PID controller coefficients, is shown in Figure 24.

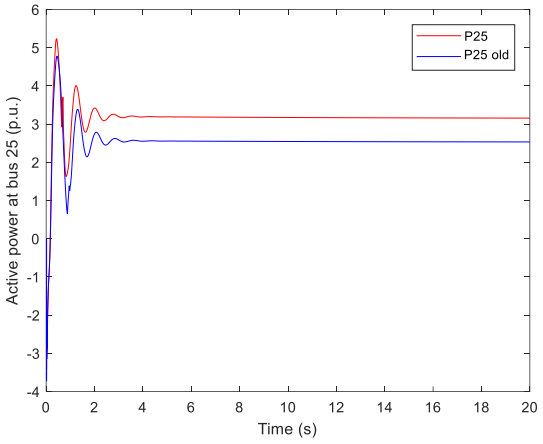

Fig. 24. Comparison of active power waveforms of the 25 kV bus in the hybrid wind farm with and without the PID controller.

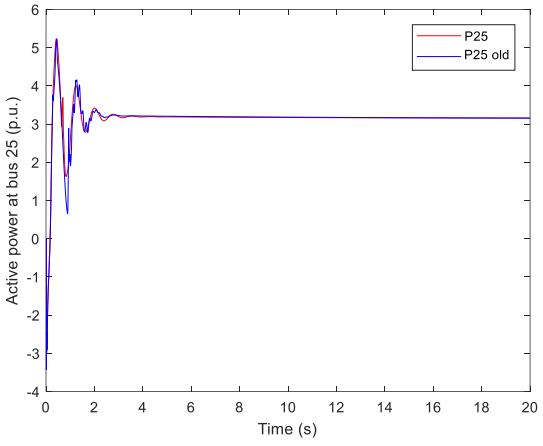

Fig. 25. Active power waveforms of the 25 kV bus in the hybrid wind farm with Kp=1K_p = 1Kp=1, Ki=0.5K_i = 0.5Ki=0.5, and Kd=0.1K_d = 0.1Kd=0.1 compared to Kp=100K_p = 100Kp=100, Ki=10K_i = 10Ki=10, and Kd=1K_d = 1Kd=1.

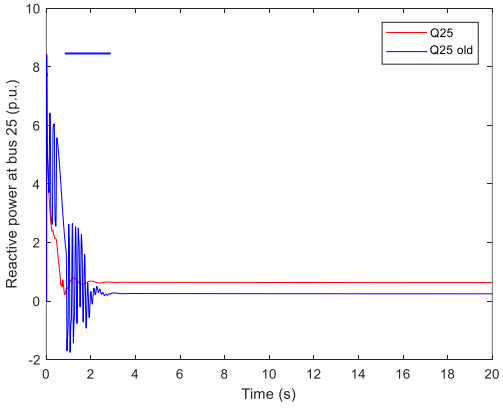

Fig. 26. Reactive power waveform of the 25 kV bus in the hybrid wind farm with Kp=1K_p = 1Kp=1, Ki=0.5K_i = 0.5Ki=0.5, and Kd=0.1K_d = 0.1Kd=0.1 compared to Kp=100K_p = 100Kp=100, Ki=10K_i = 10Ki=10, and Kd=1K_d = 1Kd=1.

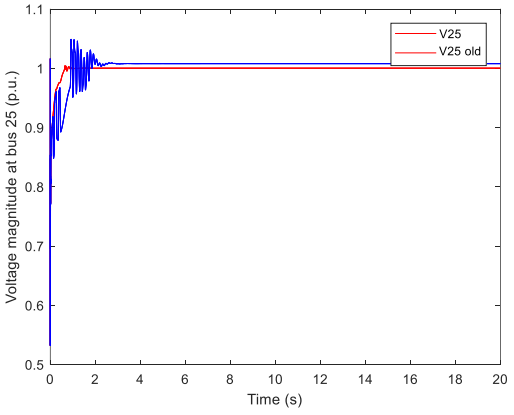

Fig. 27. Voltage waveform of the 25 kV bus in the hybrid wind farm with Kp=1K_p = 1Kp=1, Ki=0.5K_i = 0.5Ki=0.5, and Kd=0.1K_d = 0.1Kd=0.1 compared to Kp=100K_p = 100Kp=100, Ki=10K_i = 10Ki=10, and Kd=1K_d = 1Kd=1.

It is important to note that appropriate values must be chosen for the PID controller coefficients. In Figures 25 to 27, the system variable changes are compared for two sets of PID controller coefficient values. To obtain the optimal coefficients for this supplemental controller, the Particle Swarm Optimization (PSO) algorithm can be utilized.

3. OPTIMAL TUNING OF PID CONTROLLER COEFFICIENTS USING THE PARTICLE SWARM OPTIMIZATION (PSO) ALGORITHM

To optimize the PID controller coefficients using the PSO algorithm, a connection between the Simulink environment and the MATLAB environment must first be established. Then, by calling the simulations and using the necessary commands, the optimal values can be obtained.

4.1. PSO Algorithm Steps

The steps of the PSO algorithm can be summarized as follows:

1. Create the initial population and evaluate it.
2. Determine the best personal memory and the best collective memory.
3. Update velocity and position, and evaluate the new responses.
4. If the stopping criteria are not met, return to step 2.
5. End.

The stopping criteria can be, for instance, achieving an acceptable response level or reaching a predefined number of iterations.

In this study, the objective function in the PSO algorithm is to minimize the oscillations in active and reactive power following a disturbance in the system. Based on this, the optimal PID controller coefficients were determined. To find the optimal coefficients for different operating points of the system using the PSO algorithm, the power values of the dynamic and static loads (i.e., **PLD** and **PLS**) were varied.

As an example, in this study, **PLS = 1151226.38 W** and **PLD = 2472711.75 W** were assumed, and the optimal PID controller coefficients were determined to be:

Kp=1.69, Ki=4.08, Kd=0.1

In Figures 28 and 29, for the aforementioned operating point, the active power variations are compared using both the optimal coefficients for the PID controller parameters and non-optimal coefficients for the same controller.

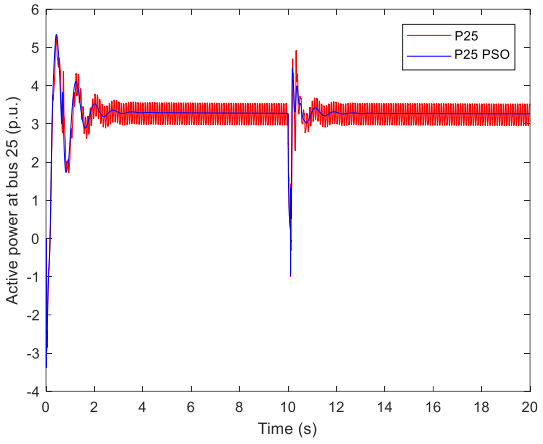

Fig. 28. Active power waveform of the 25 kV bus in the hybrid wind farm with optimized coefficients using the PSO algorithm compared to Kp=15, Ki=10, and Kd=10 at the operating point.

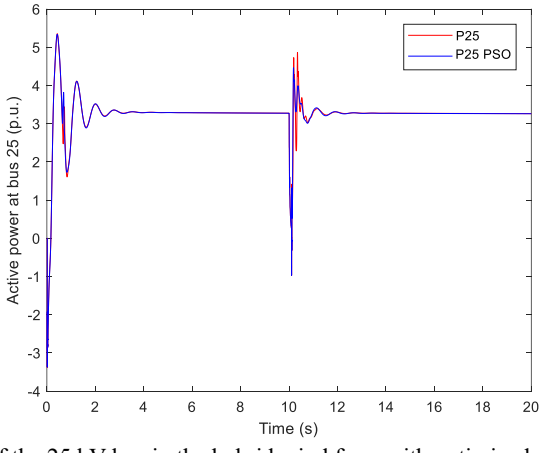

Fig. 29. Active power waveform of the 25 kV bus in the hybrid wind farm with optimized coefficients using the PSO algorithm compared to K_p=15, K_i=10, and K_d=0.01 at the operating point.

It should be noted that the performance of the PID controller is influenced by the operating conditions of the system. In other words, the optimal coefficients for the PID controller, calculated using the PSO algorithm for a specific operating point, can only enhance the system's dynamic behavior under that particular operating point. Therefore, when the system's operating conditions change, the optimal parameters of the PID controller must be recalculated using the PSO algorithm. However, finding the optimal coefficients with the PSO algorithm is time-consuming and unsuitable for real-time applications. Hence, a computational intelligence-based method, such as neural networks, is employed for the rapid estimation of the PID controller parameters, as explained in the following section.

5. REAL-TIME TUNING OF PID CONTROLLER COEFFICIENTS USING MULTILAYER PERCEPTRON (MLP) NEURAL NETWORKS

Artificial neural networks offer an intelligent and practical solution for the real-time estimation of the optimal PID controller parameters. To achieve this, the optimal PID controller parameters are first determined offline using the PSO algorithm for various system operating points. The resulting responses are then used as training patterns to

train a neural network. Once trained, the neural network can rapidly estimate the optimal PID controller coefficients when the system's operating conditions change.

5.2. Methodology for Obtaining Neural Network Training Data

5.2.1. Defining Inputs, Outputs, and Training the Neural Network

In this study, it is assumed that in the simulated system in Simulink, the power generated by the wind turbines is constant, and only the power of the two loads (one static and one dynamic) varies. By varying the load power within a specific range and using the PSO algorithm with a defined objective function for optimization, the optimal PID controller coefficients were determined.

As shown in Figure 30, the static load power (**PLS**) and the dynamic load power (**PLD**) are used as the inputs to the neural network, while the optimal PID controller coefficients (K_p, K_i, and K_d) are considered as the outputs of the MLP neural network.

The reason for selecting **PLS** and **PLD** as neural network inputs is that the power values of these two loads are directly accessible from the system. Thus, after training the neural network, the optimal PID controller coefficients for any operating point of the system can be quickly and accurately estimated in real time using only the load power values.

To ensure higher precision, three separate neural networks are used to estimate each of the three PID controller parameters.

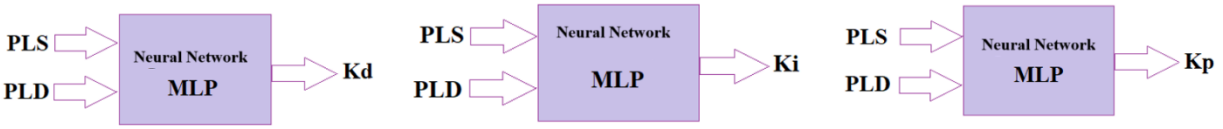

Fig. 30. Inputs and Outputs of the Three Neural Networks

5.2.2. Pattern Generation for Neural Network Training

Given the number of inputs and outputs described earlier, it can be concluded that the structure of the MLP neural network should consist of 2 neurons in the input layer, 3 neurons in the output layer, and a number of neurons in the hidden layer. As mentioned previously, in this study, three different neural networks were used to estimate the three PID controller gains, with each neural network having 2 input neurons and 1 output neuron. Each of these networks used a single hidden layer with 10 neurons. The Levenberg-Marquardt fast training method was applied to train these networks [15].

To modify the operating points of the system, it was assumed that the static load power (**PLS**) and the dynamic load power (**PLD**) could each change within a specified range around their nominal values. Random values were selected for each of these two powers within their respective variation ranges, and a random operating point for the system was generated. For each random operating point, the optimal PID controller coefficients were determined using the PSO algorithm. The variation ranges for the system loads and their nominal values are as follows:

1. The static load varies between 0.6 and 0.8 of its nominal value (**PLSr = 200 kW**).
2. The dynamic load varies between 0.5 and 0.8 of its nominal value (**PLDr = 500 kW**).

The power consumption of the static load was scaled to **1,200,000 W** (6 times its nominal power), and the dynamic load was scaled to **250,000 W** (5 times its nominal power) to allow for training with smaller values, essentially normalizing the input patterns.

Using this method, a total of 60 patterns were generated for training the neural network. Typically, 60-70% of these patterns are used for training the neural network, and the remaining 30-40% are used for testing the trained network. In this case, 42 patterns were used for training, 9 patterns were used for validation to avoid overfitting, and 9 patterns were used for testing the neural network.

5.3. Simulation Results

5.3.1. Neural Network Training and Testing Results

As discussed earlier, three neural networks were used to estimate the three PID controller gains. However, the input-output patterns were normalized before being fed into the neural network to ensure they all fell within the range of [-1, 1]. Figure 31 illustrates the training process of one of the neural networks designed using the Neural Network Toolbox of MATLAB software.

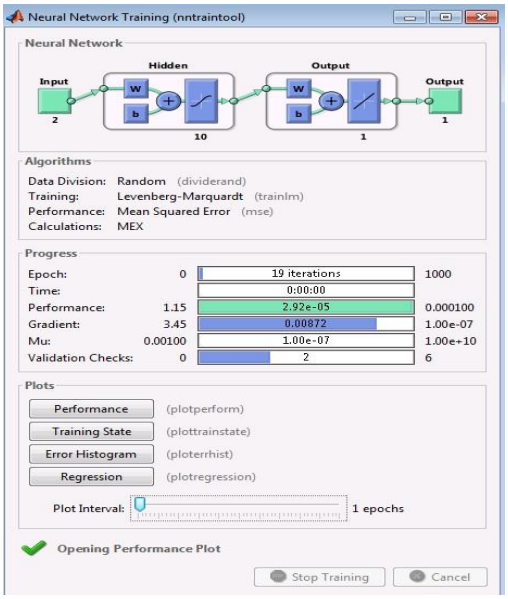

Fig. 31. Training process of the neural network for the K_P gain.

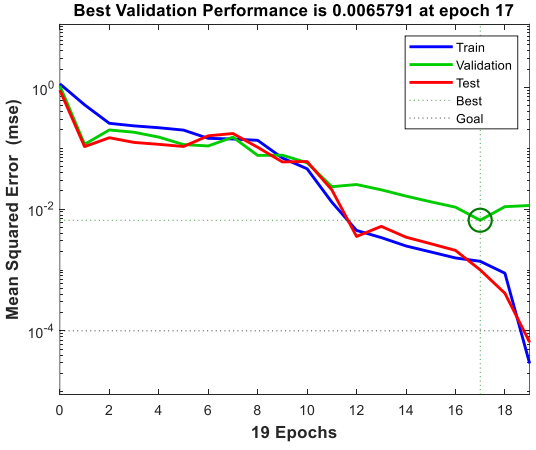

Fig. 32. Neural network learning curve for the K_P gain (using the LM method).

In Figure 32, the learning curve of the neural network for the PID controller gain Kp is shown using the Levenberg-Marquardt (LM) method. As seen from the figure, the neural network was trained over 17 epochs. In Figure 33, the learning curve of the neural network for the PID controller gain Ki is displayed. From this figure, it can be observed that the neural network was trained over 10 epochs. Similarly, in Figure 34, the learning curve of the neural network for the PID controller gain Kd is shown, illustrating the training process for this specific gain. These learning curves indicate the convergence and performance of the neural networks in estimating the PID controller gains for the system.

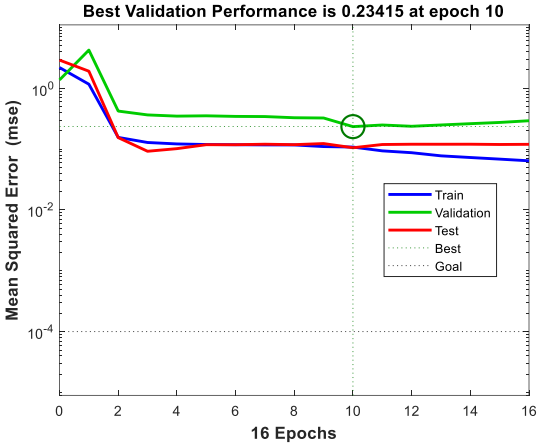

Fig. 33. Neural network learning curve for the $\mathbf{K_i}$ gain (using the LM method).

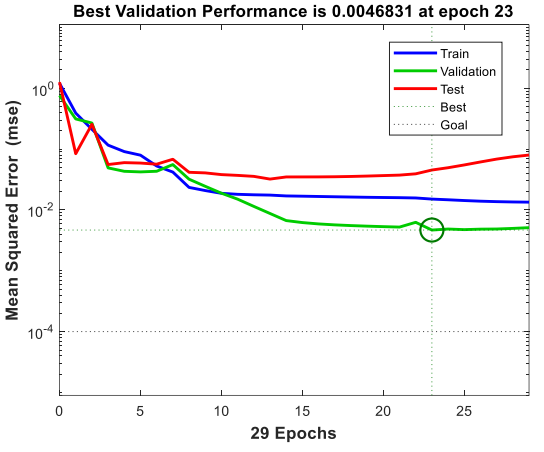

Fig. 34. Neural network learning curve for the $\mathbf{K_d}$ gain (using the LM method).

To better illustrate the input variations of the neural network, Figure 35 shows the changes in the inputs for 20 operating points of the system. This figure demonstrates that, as expected, the inputs to the neural networks are not constant.

To assess the generalization capability of the trained neural networks, their performance was evaluated using test patterns. The Root Mean Square Error (RMSE) values for the 9 test patterns corresponding to the three neural networks estimating the PID coefficients Kp**,** Ki**,** and Kd were found to be **0.0311**, **0.0631**, and **0.0330**, respectively. These values confirm that the trained neural networks are able to estimate the PID controller coefficients with good accuracy.

To further visualize this, Figures 36 to 38 compare the actual and estimated values of each of the PID controller coefficients for the test patterns. These figures clearly show that the designed neural networks have a satisfactory level of accuracy in estimating the PID controller parameters.

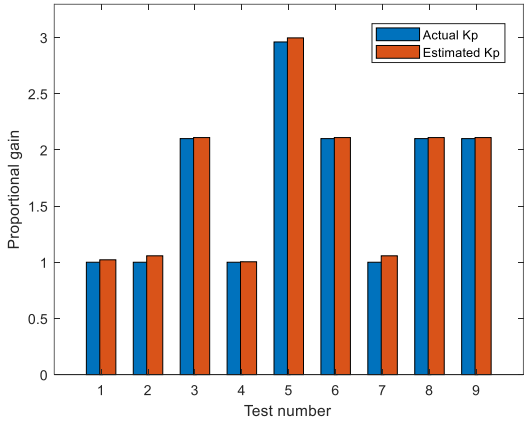

Fig. 35. Input variation method of the neural network

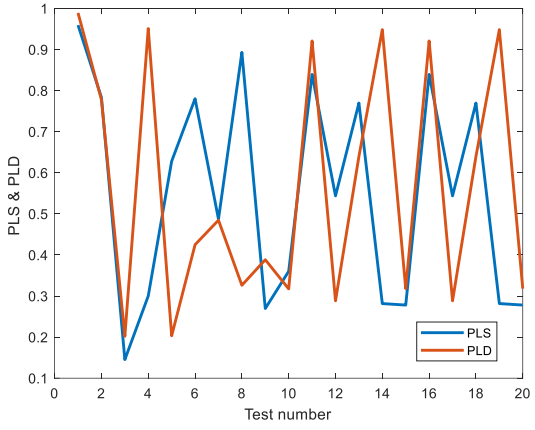

Fig. 36. Comparison of the actual value and the estimated value of the K_p parameter (with RMSE=0.0311)

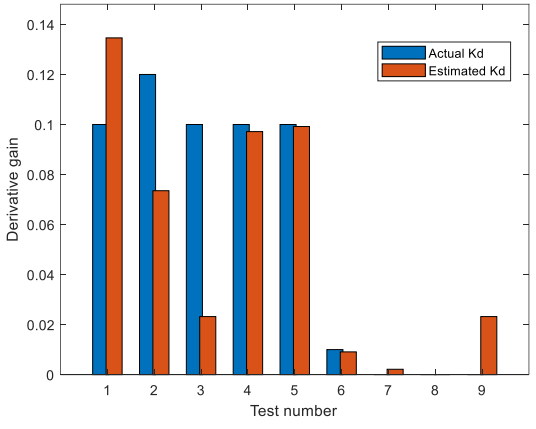

Fig. 37. Comparison of the actual value and the estimated value of the K_i parameter (with RMSE=0.6311)

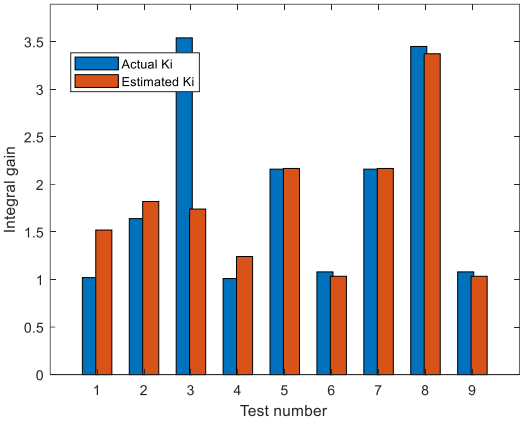

Fig. 38. Comparison of the actual value and the estimated value of the K_d parameter (with RMSE=0.0330)

6. CONCLUSION

In this article, the dynamic performance of a power system connected to a combined wind farm (CWF) was thoroughly investigated. A combined wind farm consists of both SCIG and DFIG induction generators, utilizing the advantages of both types. In such wind power plants, the reactive power injected by the DFIG converters is used to compensate for the reactive power required by the SCIG generators. However, simulation results indicated that a combined wind farm does not exhibit suitable dynamic behavior when encountering various faults.

To address this, a STATCOM was employed to compensate the system and dampen the oscillations of system variables. Moreover, it was found that for the STATCOM to improve system behavior effectively, an auxiliary controller needs to be integrated into its structure. To this end, a PID auxiliary controller was also used in the system. Additionally, simulation results demonstrated that for the auxiliary controller to operate successfully, its coefficients must be determined using one of the heuristic optimization methods, such as PSO, in response to changes in the system's operating conditions. However, determining the optimal coefficients of the auxiliary controller using the PSO algorithm is highly time-consuming.

Thus, to estimate the parameters of the auxiliary controller quickly and in real time under different operating conditions of the system, a multilayer perceptron (MLP) neural network was utilized in this study. The simulation results confirmed the successful performance of the proposed auxiliary controller and the trained neural network.

Transparency Statement

The data supporting this study are available upon reasonable request to the corresponding author, subject to ethical and confidentiality considerations.

Acknowledgments

We would like to express our gratitude to all individuals who contributed to this project.

Declaration of Interest

The authors declare that they have no competing interests.

Funding

This research received no specific grant from any funding agency, commercial, or not-for-profit sectors.

REFRENCESS

[1] R. Sadiq, Z. Wang, C.Y. Chung, C. Zhou, and C. Wang, "A review of STATCOM control for stability enhancement of power systems with wind/PV penetration: existing research and future scope", International Transactions on Electrical Energy Systems, Vol. 31, Issue 11, 2021.

[2] J. Bhukya and V. Mahajan, "Parameter tuning of PSS and STATCOM controllers using genetic algorithm for improvement of small-signal and transient stability of power systems with wind power", International Transactions on Electrical Energy Systems, Vol. 31, Issue 7, 2021.

[3] S. Kamel, F. Jurado, A. Rashad, Y. Ibrahim, and L. Nasrat, "Performance enhancement of wind farms using tuned SSSC based on artificial neural network", International Journal of Interactive Multimedia and Artificial Intelligence, Vol. 5, pp. 118-124, 2019.

[4] L. Wang and W. Huang, "Dynamic-stability enhancement and reactive power/voltage control of a large-scale wind farm using a STATCOM", IEEE North American Power Symposium, pp. 1-8, USA, 2010.

[5] A. Rashad, S. Kamel, F. Jurado and M. Abdel-Nasser, and K. Mahmoud, "ANN-based STATCOM tuning for performance enhancement of combined wind farms", Electric Power Components and Systems, Vol. 47, pp. 10-26, 2019.

[6] Liu, J., Yao, W., Wen, J., Fang, J., Jiang, L., He, H., & Cheng, S. (2020). Impact of Power Grid Strength and PLL Parameters on Stability of Grid-Connected DFIG Wind Farm. IEEE Transactions on Sustainable Energy, 11, 545-557. http://doi.org/10.1109/TSTE.2019.2897596

[7] Wang, L., & Hsiung, C.-T. (2011). Dynamic Stability Improvement of an Integrated Grid-Connected Offshore Wind Farm and Marine-Current Farm Using a STATCOM. IEEE Transactions on Power Systems, 26, 690-698. http://doi.org/10.1109/TPWRS.2010.2061878

[8] Zhang, S., Mishra, Y., & Shahidehpour, M. (2016). Fuzzy-Logic Based Frequency Controller for Wind Farms Augmented With Energy Storage Systems. IEEE Transactions on Power Systems, 31, 1595-1603. http://doi.org/10.1109/TPWRS.2015.2432113

[9] Alimi, O. A., Ouahada, K., & Abu-Mahfouz, A. (2020). A Review of Machine Learning Approaches to Power System Security and Stability. IEEE Access, 8, 113512-113531. http://doi.org/10.1109/ACCESS.2020.3003568

[10] Wang, Q., Li, F., Tang, Y., & Xu, Y. (2019). Integrating Model-Driven and Data-Driven Methods for Power System Frequency Stability Assessment and Control. IEEE Transactions on Power Systems, 34, 4557-4568. http://doi.org/10.1109/TPWRS.2019.2919522

[11] Mokhtari, M., & Aminifar, F. (2014). Toward Wide-Area Oscillation Control Through Doubly-Fed Induction Generator Wind Farms. IEEE Transactions on Power Systems, 29, 2985-2992. http://doi.org/10.1109/TPWRS.2014.2309012

[12] Arya, Y., Kumar, N., Dahiya, P., Sharma, G., Çelik, E., Dhundhara, S., & Sharma, M. (2021). Cascade-IλDμN Controller Design for AGC of Thermal and Hydro-Thermal Power Systems Integrated With Renewable Energy Sources. IET Renewable Power Generation. http://doi.org/10.1049/RPG2.12061

[13] Hasanien, H., & El-Fergany, A. (2017). Symbiotic Organisms Search Algorithm for Automatic Generation Control of Interconnected Power Systems Including Wind Farms. IET Generation Transmission & Distribution, 11, 1692-1700. http://doi.org/10.1049/IET-GTD.2016.1245

[14] Bin Wu, Yongqiang Lang, Navid Zargari, Samir Kouro, “POWER CONVERSION AND CONTROL OF WIND ENERGY SYSTEMS”, Wiley-IEEE Press, September 2011, 978-1-118-02898-8.

[15] Z. -W. Huang, G. W. Chang, I. Li, P. -G. Wang and T. K. Nguyen, "A Study of Voltage Ride-through Capability of an Offshore Wind Farm During Grid Fault Considering STATCOM Enhancement," 2021 IEEE International Future Energy Electronics Conference (IFEEC), Taipei, Taiwan, 2021, pp. 1-5, doi: 10.1109/IFEEC53238.2021.9661861.